NANO LETTERS
Cite This: Nano Lett. 2019, 19, 9145−9153
Letter
pubs.acs.org/NanoLett

One-Pot Species Release and Nanopore Detection in a Voltage-Stable Lipid Bilayer Platform

Xinqi Kang,[†,∥] Mohammad Amin Alibakhshi,[‡,∥] and Meni Wanunu*[,‡,§]

[†]Department of Bioengineering, [‡]Department of Physics, and [§]Department of Chemistry and Chemical Biology, Northeastern University, Boston, Massachusetts 02115, United States

Supporting Information

ABSTRACT: Biological nanopores have been used as powerful platforms for label-free detection and identification of a range of biomolecules for biosensing applications and single molecule biophysics studies. Nonetheless, high limit of detection (LOD) of analytes due to inefficient biomolecular capture into biological nanopores at low voltage poses practical limits on their biosensing efficacy. Several approaches have been proposed to improve the voltage stability of the membrane, including polymerization and hydrogel coating, however, these compromise the lipid fluidity. Here, we developed a chip-based platform that can be massively produced on a wafer scale that is capable of sustaining high voltages of 350 mV with comparable membrane areas to traditional systems. Using this platform, we demonstrate sensing of DNA hairpins in α-hemolysin nanopores at the nanomolar regime under high voltage. Further, we have developed a workflow for one-pot enzymatic release of DNA hairpins with different stem lengths from magnetic microbeads, followed by multiplexed nanopore-based quantification of the hairpins within minutes, paving the way for novel nanopore-based multiplexed biosensing applications.

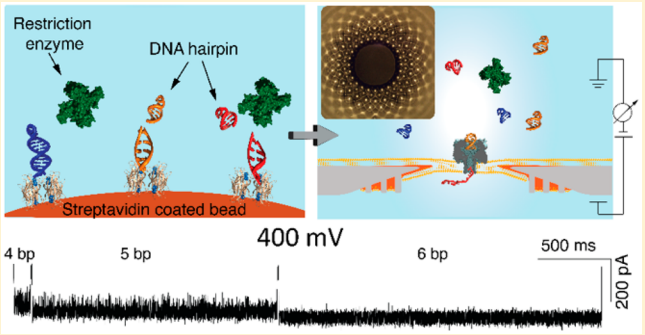

KEYWORDS: *DNA Hairpin, α-hemolysin, stable lipid bilayer, multiplexed biosensing*

Among the existing single-molecule sensing technologies, nanopores are versatile, low-cost, and label-free biosensors that have been used for a variety of applications, including DNA sequencing,[1−4] biophysical studies,[5−10] sensing RNA,[11,12] peptides,[13−15] and proteins,[16−18] studying DNA−protein[19] and protein−protein interactions[20] and measuring enzyme activity.[21−23] Biological nanopores are channels composed of either proteins or DNA origami structures[24,25] that self-assemble and insert into a lipid bilayer or polymer membrane.[26,27] Compared with their solid-state counterparts, biological nanopores are more structurally reproducible and easier to produce at large scales and have already shown great potential for DNA sequencing and biosensing applications. In order to pass molecules through them, biological nanopores usually insert into a lipid bilayer membrane which separates two chambers filled with an electrolyte solution. Applying a voltage bias across the pore results in a steady-state ion current with a flux that is limited by the pore constriction, such that a highly localized electric field is produced. When a biomolecule is captured by the electric field, the current flux is partially blocked by the presence of the biomolecule, resulting in a current blockade that corresponds to the molecule's size, charge, and conformation.

Although many different classes of molecules and biopolymers have been sensed using nanopores, typically the pore chemistry and geometry must be adapted to sense each class of analytes. For example, short nucleic acids such as microRNAs (miRNAs) translocate the pore at a time scale that requires very high bandwidths to measure, whereas on the other hand proteins are typically too large and only can traverse the pores in their fully denatured form. In order to develop a universal sensing strategy that is suitable for detecting a wide range of target molecules in nanopores (e.g., nucleic acids, protein biomarkers, metabolites, drugs, and biomolecular complexes), one approach is to indirectly sense the target analyte by sensing a surrogate molecule that reports the presence and concentration of a certain target analyte in the sample. The reporter molecules must be detectable with the nanopores in a multiplexed fashion, that is, to produce distinct signature ionic current signals while traversing a pore. In the pioneering work by Vercoutere et al.[28] it was shown that individual DNA hairpins that differ only by a single base pair in their stem length can be discriminated in α-hemolysin nanopores based on signals they produce during their accommodation in the pore vestibule. Key to this resolution and efficient detection of short hairpins is their long-lived residence times in the pore, which is orders of magnitude slower than the passage times of single-stranded DNA molecules of similar lengths through the

Received: October 28, 2019
Revised: November 12, 2019
Published: November 14, 2019

DOI: 10.1021/acs.nanolett.9b04446
Nano Lett. 2019, 19, 9145−9153

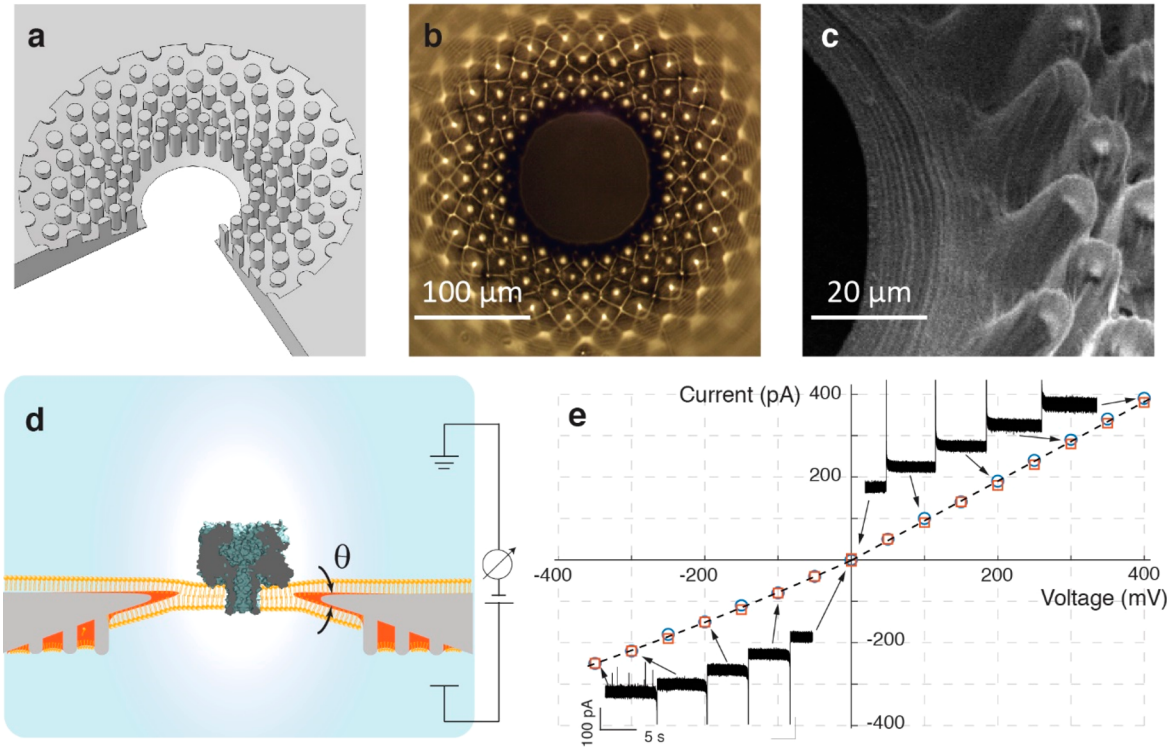

Figure 1. Pillars-on-wedge SU-8 aperture support for lipid bilayers. (a) Schematic cut-out, (b) microscope image, and (c) SEM image of a wedge-shaped aperture with pillars. (d) The lipid bilayer structure and the expected annulus shape in this aperture (aperture angle of $\theta \sim 25-30°$). (e) Current−voltage curves of two different α-hemolysin pores inserted in a DPhPC lipid bilayer in the voltage range $-350 < V < +400$ mV (1 M KCl, 20 mM Tris, pH 7.6). Insets show current traces of an α-hemolysin pore at different voltages as indicated by arrows (time and amplitude scale bars provided).

α-hemolysin pore constriction. Therefore, the DNA hairpins are prime candidates to serve as reporter molecules in a universal sensing scheme. For example, a typical affinity assay can be designed through various mechanisms that include Watson−Crick base pairing for nucleic acid target molecules or sandwich enzyme-linked immunosorbent assay (ELISA) for various antigens (e.g., protein biomarkers). In the ELISA example, antibody-functionalized beads would capture antigens, and a second antibody linked to reporter hairpins would be then bound to the antigen to form a sandwich complex. Release of these hairpins followed by their detection using a nanopore would then identify the presence and concentration of the target analyte, with the advantage being that the reporter molecule properties (size, charge) is independent from the antigen properties. Nevertheless, the first step of developing a method for reliable release and detection of reporter hairpins is essential for development of this general assay.

Here we show using a set of hairpins with designed sequences that through an efficient restriction enzyme step, DNA hairpins can be cleaved and released from magnetic microbeads. We have designed long DNA hairpins with restriction sites located at different distances from the loop, and conjugated them to magnetic microbeads through streptavidin−biotin binding. Upon cleavage with a restriction enzyme, DNA hairpins of different length are released into the buffer and detected by a nanopore without any further sample preparation and purification. In order to improve the detection sensitivity and ensure hairpin unzipping, we devised a novel chip-based lipid bilayer support platform with improved lifetimes and higher voltage stability than traditional PTFE apertures, allowing efficient sensing of released hairpins down to nanomolar (nM) concentrations. Utilizing grayscale photolithography (GPL), we fabricated ∼100 μm wide apertures in SU-8 films that have different 3D profiles. These apertures allow the convenient formation of large-area lipid bilayer membranes for single-channel measurements, as we show here for α-hemolysin recordings, that are stable for up to 8 h and routinely sustain applied voltages of 350 mV.

Stable Lipid Bilayer on SU-8 Apertures. A major drawback of biological nanopores is the fragility of the lipid bilayer membranes that support them. Traditionally, a 10−50 μm thick PTFE sheet with a 100−200 μm diameter hole drilled by laser, electrical spark ablation, or mechanical punching is used as an aperture support for lipid bilayer membranes.[29−32] Generally, the geometries and edge shapes of apertures fabricated using these relatively coarse drilling processes are not accurate and reproducible, often leading to film fragility, inhomogeneous lipid coating, low lipid membrane formation success rate, and short membrane lifetimes.[33] There are a few major avenues for improving the stability of the freestanding membranes: (i) reinforcement of the membrane by replacing biological lipids with synthetic polymers[26,27,34−37] or by strengthening the lipid bilayer through, for example, chemical conjugation of actin filaments to the bilayer,[38] (ii) support or encapsulation of the lipid bilayer by porous hydrogels,[39−43] and (iii) improved geometry and surface properties of the aperture.[33,44−46] Unlike the first two approaches, which may hinder protein insertion and biomolecule capture, modifying the aperture does not interfere with protein−membrane interactions and does not compromise analyte capture, because the native environment of the protein channel is preserved. Further, decreasing the aperture

DOI: 10.1021/acs.nanolett.9b04446
Nano Lett. 2019, 19, 9145−9153

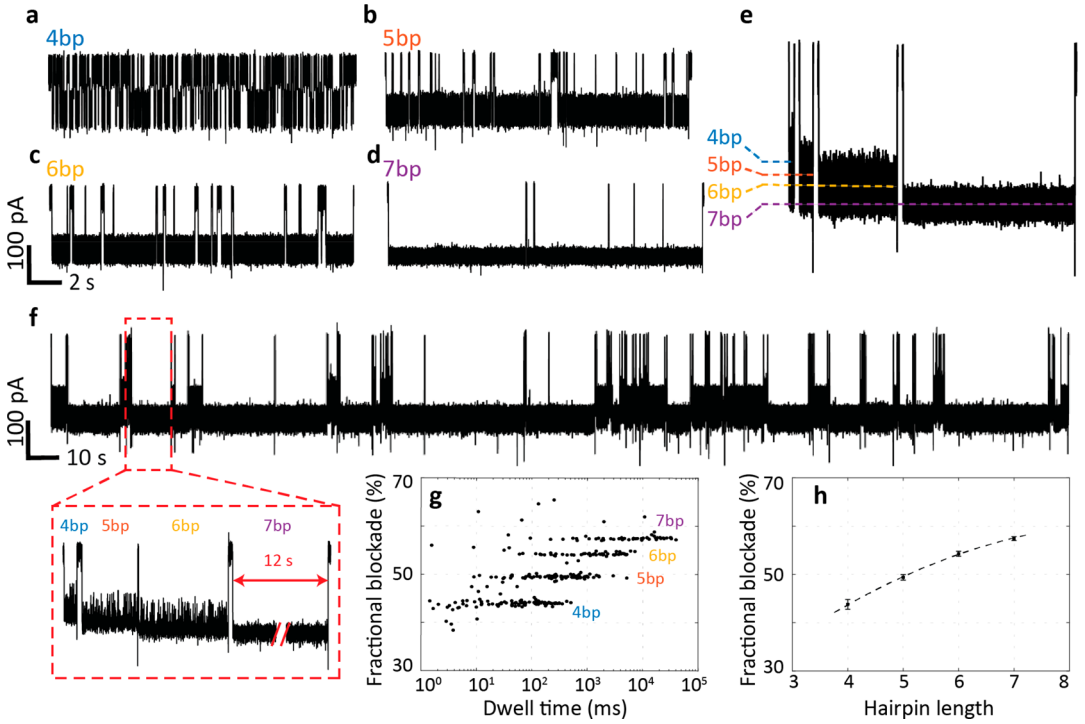

Figure 2. Differentiation of DNA hairpins with different lengths using α-hemolysin nanopores. The ionic current traces of translocation of DNA hairpins of lengths (a) 4, (b) 5, (c) 6, and (d) 7 bp through α-hemolysin nanopore at 1 μM hairpin concentrations. (e) Representative translocation events produced by different hairpin lengths (dashed lines indicate the mean current levels obtained for the different hairpins). (f) Continuous current versus time trace (350 s) showing capture and translocation of a mixture of 4−7 bp hairpins, (g) scatter plot of fractional blockade versus dwell time for the four-hairpin mixture, and (h) mean fractional current blockade versus hairpin length for the data from (g). The concentrations of each DNA hairpin in the mixture was 250 nM. All measurements were performed with 1 M KCl, 20 mM Tris, and pH 7.6 at 300 mV applied bias.

diameter[31,44] can further improve the membrane stability, although this compromises the protein channel insertion probability, especially for protein channels that are delivered by proteoliposomes.[33,47] Another strategy previously reported to improve the stability of lipid membranes is to use thinner apertures[48] or alternatively creating an aperture with sharper edges[33,46] which allows the two lipid leaflets across the aperture to meet each other over a smoother curve, thereby forming a bilayer with minimum perturbations caused by solvent annulus fluctuations.[46,48]

Here, we have developed a method for scaled-up fabrication of such apertures with sharp edges using GPL. SU-8 is a hydrophobic polymer with low dielectric constant, which makes it a suitable material for lipid bilayer membrane apertures.[33,46,49] Furthermore, its compatibility with standard photolithography and its availability in thin layer format (2−200 μm) enables a range of structures to be fabricated. The main advantage of an SU-8 aperture over commonly used PTFE apertures is its smoother edges, as well as the excellent control over the diameter and thickness of the aperture afforded by the GPL process. We note two important aspects of forming a stable lipid bilayer support: (1) it benefits from a small merging angle (θ) of the two leaflet layers, and (2) solvent drainage during the experiments destabilizes the membrane. We further note that due to geometrical constraints, the commonly used cylindrical apertures suffer from a relatively large merging angle (Figure S1a−d).[46] We addressed this problem by taking advantage of GPL to effectively produce a UV exposure dose gradient[50] at the aperture, thereby controlling its edge thickness and slope. The resulting apertures with wedge-shaped cross sections (Figure S1e−h) are expected to outperform cylindrical apertures, because the two lipid leaflets from the top and bottom of the solvent annulus merge smoothly with a smaller angle and a minimum perturbation. Moreover, membrane stability could be further improved by creating structures around the wedge-shaped aperture that provide a solvent reservoir to compensate for its drainage during prolonged experiments. Therefore, we used GPL to fabricate a wedge-shaped aperture surrounded by solvent-pinning pillars. In Figure 1a−c, we show a schematic drawing, optical microscope image, and scanning electron microscope image of this aperture, respectively. The pillars' diameters and spacing are designed to provide an inward capillary force toward the aperture edge (Figures 1a). The photomask patterns used for fabricating the wedge-shaped and the pillars-on-wedge aperture are depicted in Figure S2. All three apertures have been fabricated on a 20 μm thick SU-8 layer with a target aperture diameter of 100 μm, although sometimes we obtained slightly larger (<10%) final diameters due to underexposure of the patterns.

Previous studies indicate that α-hemolysin nanopores do not gate at applied voltages below 340 mV, and therefore these channels are prime candidates for high-voltage sensing applications.[51] We tested the stability of membranes formed on our SU-8 supports by inserting a single α-hemolysin channel into diphytanoylphosphatidylcholine (DPhPC) lipid bilayers. Table S1 summarizes the performance of the lipid bilayers suspended on the three aperture types under high applied bias. The overall performance of the pillars-on-wedge was observed to be superior to the other apertures, and we

DOI: 10.1021/acs.nanolett.9b04446
Nano Lett. 2019, 19, 9145−9153

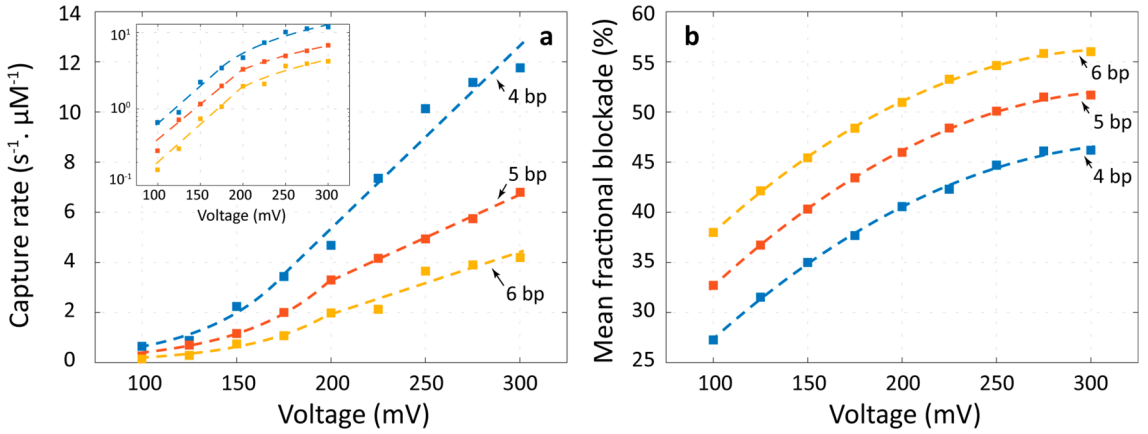

Figure 3. (a) Voltage-dependent concentration-normalized capture rates for 4bp, 5bp, 6bp DNA hairpins. Inset to panel a shows a semilog representation of the data, highlighting the Arrhenius capture regime at low voltage and the diffusion-governed regimes at high voltages. b) Mean fractional current blockade for the same hairpins. A second order polynomial was used to fit the data, represented by the dashed lines. All measurements were performed in 1 M KCl, 20 mM Tris, pH 7.6, and each hairpin concentration was 100 nM.

consistently were able to apply 350 mV applied bias across bilayers formed in such apertures. Further, we use this platform to show that α-hemolysin does not gate at voltages as high as 400 mV, as indicated by the current−voltage curve shown for two different channels in Figure 1e (current trace at 400 mV shown in Figure S3), whereas for negative bias gating occurs at values of −350 mV, as evidenced by the spikes in the current trace (Figure 1e, inset). Although we were able to record at 400 mV, we often observe leakage current in some of our devices, as evidenced by increased current baselines and current fluctuations. Nevertheless, we found that the pillars-on-wedge apertures were more stable than the wedge and cylindrical apertures, which withstood lower voltages of 300 and 250 mV, respectively, before exhibiting leakage currents and membrane instability. To our knowledge, the voltage stability of the cylindrical structure is comparable to the best reported PTFE apertures with the same diameter,[31,52] whereas the edge and pillars-on-wedge apertures are superior. Further, a DPhPC lipid bilayer formed on these apertures can last for up to 8 h under <150 mV applied bias after single-channel α-hemolysin insertion. Continuous application of 300 mV applied bias breaks the DPhPC bilayer after 30 min. However, intermissions at lower voltage values resolve this problem and significantly increase the membrane's lifetime.

Nanopore Sensing of DNA Hairpins. Here we show that DNA hairpins are viable reporter molecules for multiplexed nanopore-based sensing. Unzipping dynamics of blunt end,[28] fishhook (one-tail),[53−55] and internal (two-tail) DNA hairpins[53] in α-hemolysin pores have been extensively explored at low applied voltages (<120 mV). Furthermore, hairpin structures with subtle structural differences,[53] as well as blunt hairpins with even a single nucleotide difference in the stem lengths,[28] produce differentiable current blockades. Other attractive features of DNA hairpins as reporters include their low cost, biocompatibility, thermal stability, high charge density for facilitating capture into nanopores, and, finally, their facile and efficient release into solution by cleavage using restriction enzymes. We therefore capitalize on our developed lipid bilayer support platform to investigate detection of these molecules at high applied bias, aiming to achieve a higher level of multiplexing, lower LOD values, and improved identification accuracies by enhanced signal-to-noise ratios. We further demonstrate a one-pot method for restriction enzyme mediated release of DNA hairpins from a bead and their direct identification without further purification steps.

The sequences of the DNA hairpins used in this study are shown in Figure S4a. DNA hairpin purity was first assessed using 20% native PAGE electrophoresis (Figure S5), which shows that DNA strands have folded into uniform hairpin structures. We used the pillars-on-wedge SU-8 aperture to suspend DPhPC lipid bilayer and insert a single α-hemolysin pore. Figure 2a−c shows representative current traces of 4, 5, 6, and 7 bp DNA hairpins translocating through an α-hemolysin pore at 300 mV. Comparison of single events from each hairpin length (Figure 2e) clearly shows distinct current levels and dwell times. Additionally, as previously reported, each event has a characteristic dwell time corresponding to the hairpin being trapped inside the pore vestibule, followed by a sharp deep blockade which indicates hairpin has unzipped and translocated through the pore.[28] This second level for some of the events have not been captured owing to the unzipping time scales being faster than our measurement bandwidth. We note that as the stem length increases, the current blockade increases because a larger volume inside the α-hemolysin vestibule is occupied by the hairpin stem. This was further demonstrated by examining simultaneous detection of a mixture of four different hairpin lengths. Figure 2f shows a 350 s current trace of a mixture of 4−7 bp DNA hairpins translocation through α-hemolysin recorded at 300 mV. The zoomed-in trace clearly shows four distinct current blockade levels, each associated with a different hairpin. Scatter plot of the current blockade-dwell time clearly demonstrates four distinguishable populations (Figure 2g) and confirms that multiplexed sensing with a mixture of hairpins can be done with high fidelity. Moreover, this plot indicates longer hairpins dwell inside the vestibule for longer times, which points to a higher energy required for unzipping. The large standard deviation of the dwell time distribution evident from the scatter plot is a characteristic of the hairpin unzipping dynamics. Mean fractional current blockades for different DNA hairpin stem lengths, obtained from Gaussian fits, indicates a relationship between fractional blockade and the hairpin length that is best described by a second-order polynomial (Figure 2h, dashed line).

We also investigate the possibility of unzipping longer hairpins in α-hemolysin nanopores, as it was previously shown

DOI: 10.1021/acs.nanolett.9b04446
Nano Lett. 2019, 19, 9145−9153

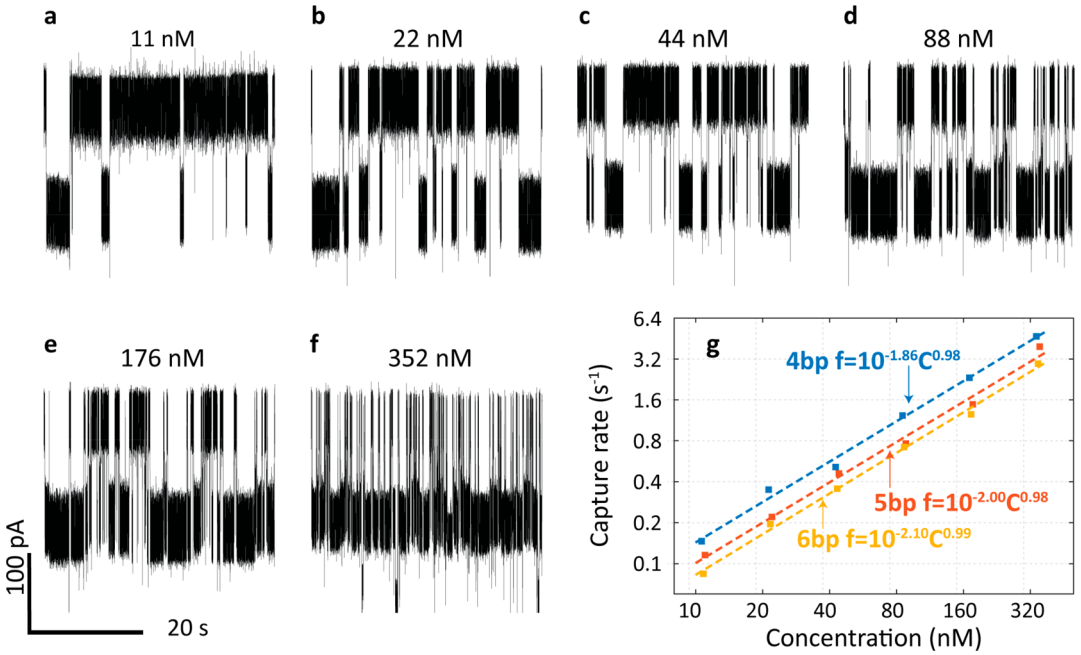

Figure 4. DNA hairpin capture rates vs concentration. (a–f) Current traces recorded with a mixture of 4, 5, and 6 bp DNA hairpins at different concentration (indicated values are for each hairpin in the mixture). (g) Capture rate as a function of hairpin concentration. Experiments were performed in 1 M KCl, 20 mM Tris, pH 7.6, at 300 mV applied bias. Current signal was lowpass filtered at 10 kHz.

that hairpins longer than 6 bp cannot translocate at 120 mV.[28] Interestingly, we observed that despite the large applied voltage, DNA hairpins longer than 6 bp still do not smoothly translocate through the pore. In case of the 7 bp hairpins, although they can traverse the pore at 300 mV, their dwell times are very long and can be up to 40 s (Figure 2g). As for the 8 bp hairpins, the stem length is close to the length of the vestibule and therefore a smaller electromotive force is applied to the loop, whereas the blunt end of the hairpins are pressed against the pore constriction. We observe the 8 bp hairpins sometimes translocate through the pore and sometimes attempt to enter the constriction but cannot translocate, giving rise to multiple current levels, very high blockades (~96%), and long dwell times (>100 s) until they are removed from the vestibule by reversing the voltage polarity (Figure S6). Therefore, in this work we restricted our multiplexing strategy to three reporter molecules, namely, 4–6 bp hairpins.

The most critical factor in developing a nanopore-based sensitive detection scheme is the capture rate of the species. Studies pertaining translocation of single-stranded DNA through α-hemolysin distinguish two different capture regimes,[56−58] namely the energy barrier-limited and the diffusion-limited regimes. At small applied bias values, an energy barrier associated with entropic and steric effects limits the entry rate of molecules into the pore. In this voltage regime, the capture rate increases exponentially with applied voltage, suggesting that capture is best described by an Arrhenius equation. In addition, in this regime we find that capture attempt rates, indicated by the offset of the semilog curves in Figure 3a, decrease with hairpin lengths. We attribute this to the smaller diffusion coefficients for longer hairpins, which in turn reduces attempt rates. However, beyond some voltage threshold, hairpin diffusion to the pore's capture zone determines the capture rate. In this regime, capture rate is linearly proportional to the voltage, consistent with the expected linear increase in capture radius with increasing bias. Our results indicate a crossover voltage of 175 mV for the 4 bp hairpin and ~200 mV for longer hairpins. This value is higher than the crossover voltage of poly$(dC)_{40}$ single-stranded DNA translocation (i.e., 120–140 mV),[56] which informs on the higher energy barrier associated with tight immobilization of the hairpins inside the pore vestibule. Nonetheless, it is clear from Figure 3a that the ability to increase the applied bias to 300 mV results in an order of magnitude improvement in capture rate for all three hairpins. These results were obtained with a mixture of hairpins in a single pore to eliminate possible pore-to-pore variation and other experimental errors. We further note that increasing the applied bias increases the mean fractional current blockades (Figure 3b). This suggests that a higher applied force can partially squeeze the hairpin loops into the vestibule. An important consequence of this is that signal-to-noise values are further enhanced at the higher voltages.

Next, we investigated the practical limits of detection for a mixture of DNA hairpins at different concentrations under high applied bias. Each hairpin had a concentration in the range of 10–350 nM. Figure 4a–f shows the current traces of translocation of hairpin mixtures with different concentrations at 300 mV. At the lowest concentration, a 10 min current recording was obtained and a total number of 210 events were detected. Capture rates were extracted by fitting exponential curves to the interevent time distributions. As the log–log plot in Figure 4g shows, we find within error a good linear dependence between capture rate and concentration for all three hairpins, with exponents of 0.98, 0.98, and 0.99 for the 4, 5, and 6 bp hairpins, respectively. Further, we consistently find that longer hairpins have lower capture rates, as evident in this plot, although the exact difference in capture rates varies from pore to pore, presumably due structure variability in the commercial version of our α-hemolysin. Importantly, under high applied voltage detection of these hairpins at few-nanomolar concentrations is practical with rates in the range of 0.1 s^{-1} for 10 nM hairpin concentrations. Finally, we note that

DOI: 10.1021/acs.nanolett.9b04446
Nano Lett. 2019, 19, 9145–9153

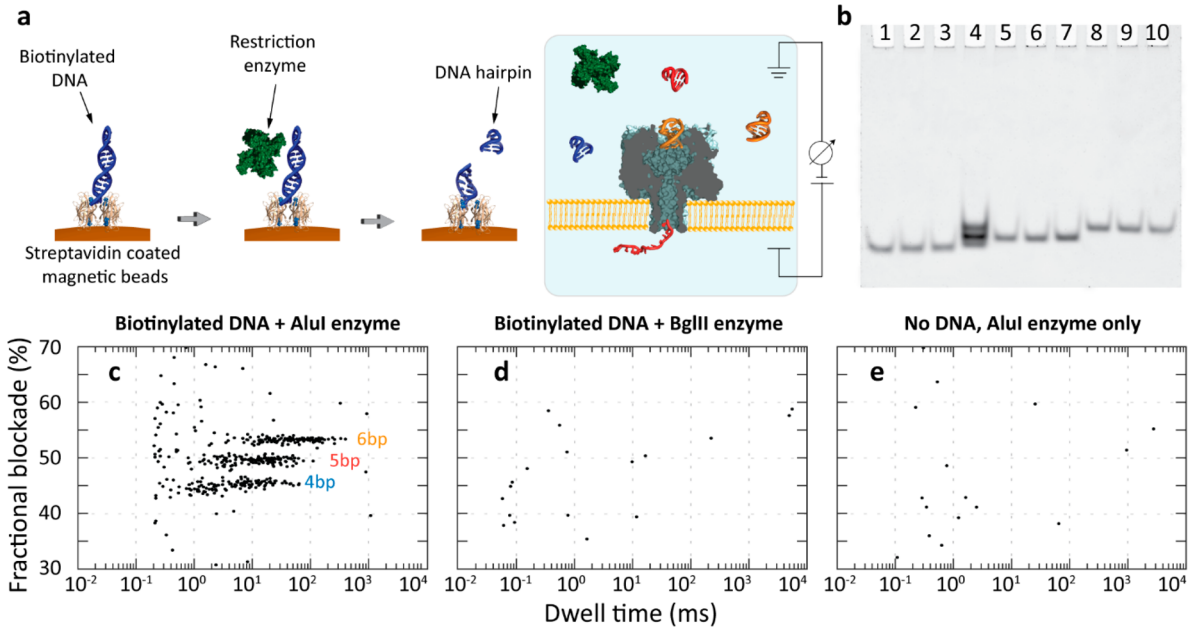

Figure 5. Enzymatic release and direct sensing of reporter hairpins. (a) Schematics of releasing DNA hairpins using a restriction enzyme and magnetic beads. (b) The 20% Native PAGE gel stained by Gelred. Lanes 1−3: 4 bp DNA hairpins cleaved using 20U, 40U, and 60U enzyme, respectively. Lane 4: mixture of 4, 5, and 6 bp DNA hairpins. Lanes 5−7: 5 bp DNA hairpin cleaved using 20U, 40U, and 60U enzyme, respectively. Lanes 8−10: 6 bp DNA hairpin cleaved using 60U, 40U, and 20U enzyme, respectively. All samples were incubated for 3 h at 37 °C. (c) Scatter plot of fractional current blockade versus dwell time obtained from analysis of a 4 min recording of a hairpin mixture cut from the beads using the AluI enzyme. (d) A negative control in which hairpins were exposed to BgIII, which does not recognize the hairpin sequences. (e) A negative control in which no DNA hairpin was immobilized on the beads. Experiments were performed at 300 mV, and the current signal was lowpass filtered at 10 kHz.

this limit can in principle be pushed further to lower practical LOD values by applying a salt gradient across the pore.

Enzymatic Release of Reporter Hairpins. Here we create a model system where hairpins immobilized on microbeads are released using a simple enzymatic cleavage step, followed by their nanopore-based detection without any purification steps. We designed a new set of longer DNA hairpins by extending 4−6 bp hairpins by 10 bp, such that cutting these extended hairpins using a restriction enzyme releases 4, 5, and 6 bp hairpins with the exact same sequences as used earlier (Figure S7). In fact, the stem end of all DNA hairpins used in the previous section were designed to match the recognition site of the restriction enzyme AluI, an enzyme that can efficiently cut DNA even close to the DNA end (Figure S4b). Further, the 5′ ends of the extended hairpins were biotinylated to allow conjugation with streptavidin-coated magnetic beads. The binding efficiency of biotinylated hairpins with the beads was confirmed to be high using PAGE (Figure S8). By introducing the enzymes, extended hairpins were cut and the reporter molecules were released from the beads (Figure 5a). Successful cutting of the hairpins was further verified using native PAGE, as shown in Figure 5b. Cutting immobilized hairpins produced bands corresponding to the 4−6 bp hairpins. Here, we note that when the restriction site is close to the bead surface, the reaction rate is reduced as compared to the free-solution rate for the same molecules (Figure S9c). For example, a free-solution reaction time of 3 h resulted in quantitative short hairpin formation using 10U enzyme (Figure S9b), whereas in contrast 60U enzyme was needed to maximize the cutting yield of hairpins from beads.

Because enzyme cutting introduces foreign species to the analyte solution, such as AluI and BSA (bovine serum albumin), we tested for potential interference of these species with the expected hairpin signals. To do this, we tested the reaction solution after enzymatic release from beads without any purification steps (Figure 5c). Importantly, we observe that despite the presence of these proteinaceous contaminants we still can reliably sense and differentiate all of the hairpins in the mixture. Data presented in this figure was obtained from a 4 min long recording, with the immobilized hairpin concentrations of C_{4bp} = 90 nM, C_{5bp} = 130 nM, and C_{6bp} = 160 nM on the beads. The measured hairpin concentrations obtained by looking up their capture rates in Figure 4, are C_{4bp} = 51 nM, C_{5bp} = 83 nM, and C_{6bp} = 95 nM which are 35−40% lower than the expected values. This suggests incomplete release of the hairpins from the beads by restriction enzymes, which requires further quantification and calibrations. However, we note here that since the hairpins are first immobilized on beads, their concentrations can be effectively increased by reducing the volume of the release solution, thereby allowing sample preconcentration for improved LOD values. An alternative approach we explored in which the reporter hairpins can be more efficiently detected employs a free-solution cutting of the hairpins, followed by uptake of the biotinylated 10 bp dsDNA stems onto streptavidin-coated magnetic beads (Supporting Information, Section IV). This method shows a high cutting efficiency and requires less enzyme units. As a negative control, we performed an analogous experiment with BgIII, an enzyme whose restriction site sequence does not match the sequence of hairpins. Nanopore measurements (10 min) shown in Figure 5d reveal rare sporadic spikes with random current blockade levels and dwell times, unlike the clear populations formed by the released DNA hairpins shown in Figure 5c. These sporadic

DOI: 10.1021/acs.nanolett.9b04446
Nano Lett. 2019, 19, 9145−9153

events, which result from protein interactions with the pore, are further exemplified by a second negative control experiment where the enzymatic reaction was performed with no DNA substrate immobilized on the beads (Figure 5e). We note that these protein-pore interactions, which only occur at 300 mV bias, are not present at a 200 mV bias.

Here we demonstrated a multiplexed biosensing scheme based on enzymatic release of reporter DNA hairpins from microbeads. Stability of the lipid bilayers on the SU-8 apertures was essential in achieving practical detection from nanomolar-level concentrations. The on-chip SU-8 apertures are conveniently and massively produced on a wafer-scale, and the chip form factor is compatible with optical measurements, for example, for optoelectronic tracking of ion channels, as well as compatible with further elaboration using lithography, for example, design of on-chip fluidics for low-volume sample analysis. Use of restriction enzymes as a scheme to release reporter molecules is not only compatible with wet-lab molecular biology assays, but also benefits from the sequence specificity and plurality of restriction enzyme choices, which enable further multiplexing. For example, an alternative multiplexing method would be to, instead of sensing different reporter molecules, use the same hairpin lengths with different cutting site sequences and release them using different enzymes. Finally, our results inspire a new modality for biochemical data storage using DNA hairpins and reading them using nanopores (Supporting Information, Section V). In this scheme, each hairpin could be viewed as a bit which can take multiple values based on its concentration. If N is the number of differentiable concentrations by the nanopore and m is the number of hairpins that can be differentiated based on their current blockade or dwell times, then a small drop of a hairpin mixture can be defined as a data byte which can assume a value between 0 to $(N^m - 1)$. Therefore, by creating a nanopore-integrated droplet manipulator, information stored in droplets of hairpin mixtures can be retrieved. Furthermore, data encryption is possible via release of hairpins with a unique restriction enzyme. This proposal can open an avenue for long-term data storage and cryptography using DNA and other nanopore-readable biomolecules.

Methods. *Fabrication of SU-8 Apertures.* The SU-8 apertures were fabricated on a 500 μm thick ⟨100⟩ Si wafer that contains a 2 μm thick wet thermal SiO_2 layer prior to coating with a 50 nm thick silicon nitride layer. The buried SiO_2 layer serves to reduce the capacitance of chips. The wafer was patterned to expose an array of 1 mm squares using standard photolithography, followed by SF_6 reactive ion etching at 150 W for 2 min to etch the silicon nitride. Next, the silicon dioxide layer was removed using buffered oxide etch (BOE) for 45 min, whereas the back side of wafer was protected from the BOE etchant using a single side etcher. A 2010 SU-8 film was spun-coat on the other side of the wafer at 1000 rpm for 60 s, soft baked at 95 °C for 5 min, and exposed with constant power at 275 W for 12 s. Grayscale photolithography was used to create wedge-shaped and pillars-on-wedge shaped apertures (Figure S2). After exposure, the wafer was postbaked at 95 °C for 5 min and developed for 4 min. Next, using a single side etcher, the silicon wafer was anisotropically etched using KOH while the wafer back side was protected, and finally the SiO_2 and the silicon nitride layers were etched with BOE for 45 min and SF_6 reactive ion etching at 150 W for 2 min.

Lipid Bilayer Painting and Nanopore Measurement. The SU-8 aperture was first pretreated with 1 μL of DPhPC (Avanti Polar Lipids) (5 mg/ml) dissolved in hexane on each side of the membrane. After the hexane evaporated, the chip was mounted on a custom designed flow cell and the cis and trans chambers were filled with 1 M KCl, 20 mM Tris, pH 7.6 electrolyte. A pair of Ag/AgCl electrodes were inserted to the chambers and connected to an Axon 200B patch-clamp amplifier to measure the ionic current. Lipid bilayer was painted across the aperture using 20 mg/ml DPhPC dissolved in decane. After lipid bilayer formation, 0.5 μL of 5 μL/ml α-hemolysin (Sigma-Aldrich) was added to the cis chamber until a single channel insertion was observed. DNA hairpin samples were added to the cis chamber and mixed gently using a pipet. Current signals were collected at sampling rates of 250 kHz, lowpass filtered to 10 kHz, and analyzed using Pythion, a software developed for analyzing nanopore signals.

Enzymatic Release of Hairpins. All oligonucleotides were purchased from Integrated DNA Technologies (IDT) and the restriction enzyme AluI was purchased from New England Biolabs (NEB). A suspension of 25 μL of 10 mg/ml magnetic beads (Dynabeads M-270 Streptavidin, Invitrogen) was transferred to a clean PCR tube and washed with 25 μL of 2X Binding&Washing Buffer (2 M NaCl, 1 mM EDTA,10 mM Tris-HCl, pH 7.5) three times with gentle pipetting. Fifty microliters of the 2X Binding&Washing was added to make the bead concentration 5 mg/ml. Next, 50 μL of 20 ng/μL DNA substrate (1 μg DNA) was added to the beads and incubated at room temperature for 30 min while gently shaking the tube using an incubated tube rotator (Roto-Therm). After DNA conjugation, beads were washed with 1X Binding&Washing Buffer two times and again once with 1X CutSmart Buffer (50 mM potassium acetate, 20 mM Tris-acetate, 10 mM magnesium acetate, 100 μg/ml BSA). The supernatant was removed and saved for a binding efficiency test. The enzyme digestion experiment was performed with 20U, 40U, and 60U AluI enzyme in 50 μL final volume of 1X CutSmart Buffer and was incubated at 37 °C for 3 h, while gently shaking. After enzyme digestion, beads were separated using a magnet, and the supernatant was mixed with the desired amount of 4 M KCl buffer (20 mM Tris, pH 7.6) so that the final KCl concentration is 1 M. DNA hairpins were characterized using 20% native PAGE. All gels were run at 150 V for 1 h, stained with Gelred, and visualized with a Biorad PharosFX imaging system.

■ ASSOCIATED CONTENT

Supporting Information

The Supporting Information is available free of charge on the ACS Publications website at DOI: 10.1021/acs.nanolett.9b04446.

The SU-8 apertures and their performance, the reporter DNA hairpins sequence, PAGE characterization, and nanopore sensing, the biotinylated DNA hairpins sequences and binding efficiency, an alternative approach to releasing the hairpins, and finally implications of hairpins multiplexed sensing for chemical data storage (PDF)

■ AUTHOR INFORMATION

Corresponding Author

*E-mail: wanunu@neu.edu.

DOI: 10.1021/acs.nanolett.9b04446
Nano Lett. 2019, 19, 9145−9153

ORCID

Meni Wanunu: 0000-0002-9837-0004

Author Contributions

‖X.K. and M.A.A. contributed equally to this work.

Notes

The authors declare no competing financial interest.

■ ACKNOWLEDGMENTS

The authors thank Zhuoyu Zhang and Xin Li for fruitful discussions and Dr. Wentao Liang for providing the SEM images. This work was supported by the National Science Foundation, Grant 1645671 (MCB).

■ REFERENCES

(1) Clarke, J.; Wu, H.-C.; Jayasinghe, L.; Patel, A.; Reid, S.; Bayley, H. *Nat. Nanotechnol.* **2009**, *4* (4), 265−270.
(2) Derrington, I. M.; Butler, T. Z.; Collins, M. D.; Manrao, E.; Pavlenok, M.; Niederweis, M.; Gundlach, J. H. *Proc. Natl. Acad. Sci. U. S. A.* **2010**, *107* (37), 16060−16065.
(3) Fuller, C. W.; Kumar, S.; Porel, M.; Chien, M.; Bibillo, A.; Stranges, P. B.; Dorwart, M.; Tao, C.; Li, Z.; Guo, W.; et al. *Proc. Natl. Acad. Sci. U. S. A.* **2016**, *113* (19), 5233−5238.
(4) Noakes, M. T.; Brinkerhoff, H.; Laszlo, A. H.; Derrington, I. M.; Langford, K. W.; Mount, J. W.; Bowman, J. L.; Baker, K. S.; Doering, K. M.; Tickman, B. I.; et al. *Nat. Biotechnol.* **2019**, *37* (6), 651.
(5) An, N.; Fleming, A. M.; Middleton, E. G.; Burrows, C. J. *Proc. Natl. Acad. Sci. U. S. A.* **2014**, *111* (40), 14325−31.
(6) Jin, Q.; Fleming, A. M.; Burrows, C. J.; White, H. S. *J. Am. Chem. Soc.* **2012**, *134* (26), 11006−11.
(7) Noakes, M. T.; Brinkerhoff, H.; Laszlo, A. H.; Derrington, I. M.; Langford, K. W.; Mount, J. W.; Bowman, J. L.; Baker, K. S.; Doering, K. M.; Tickman, B. I.; Gundlach, J. H. *Nat. Biotechnol.* **2019**, *37*, 651.
(8) Wescoe, Z. L.; Schreiber, J.; Akeson, M. *J. Am. Chem. Soc.* **2014**, *136* (47), 16582−7.
(9) Alibakhshi, M. A.; Halman, J. R.; Wilson, J.; Aksimentiev, A.; Afonin, K. A.; Wanunu, M. *ACS Nano* **2017**, *11* (10), 9701−9710.
(10) Cao, C.; Li, M. Y.; Cirauqui, N.; Wang, Y. Q.; Dal Peraro, M.; Tian, H.; Long, Y. T. *Nat. Commun.* **2018**, *9* (1), 2823.
(11) Wang, Y.; Zheng, D.; Tan, Q.; Wang, M. X.; Gu, L.-Q. *Nat. Nanotechnol.* **2011**, *6* (10), 668−674.
(12) Shasha, C.; Henley, R. Y.; Stoloff, D. H.; Rynearson, K. D.; Hermann, T.; Wanunu, M. *ACS Nano* **2014**, *8* (6), 6425−6430.
(13) Huang, G.; Voet, A.; Maglia, G. *Nat. Commun.* **2019**, *10* (1), 835.
(14) Piguet, F.; Ouldali, H.; Pastoriza-Gallego, M.; Manivet, P.; Pelta, J.; Oukhaled, A. *Nat. Commun.* **2018**, *9* (1), 966.
(15) Ji, Z.; Kang, X.; Wang, S.; Guo, P. *Biomaterials* **2018**, *182*, 227−233.
(16) Rodriguez-Larrea, D.; Bayley, H. *Nat. Nanotechnol.* **2013**, *8* (4), 288−95.
(17) Nivala, J.; Marks, D. B.; Akeson, M. *Nat. Biotechnol.* **2013**, *31* (3), 247−50.
(18) Fahie, M.; Chisholm, C.; Chen, M. *ACS Nano* **2015**, *9* (2), 1089−98.
(19) Langecker, M.; Ivankin, A.; Carson, S.; Kinney, S. R.; Simmel, F. C.; Wanunu, M. *Nano Lett.* **2015**, *15* (1), 783−90.
(20) Thakur, A. K.; Movileanu, L. *Nat. Biotechnol.* **2019**, *37*, 96.
(21) Harrington, L.; Alexander, L. T.; Knapp, S.; Bayley, H. *ACS Nano* **2019**, *13*, 633.
(22) Harrington, L.; Alexander, L. T.; Knapp, S.; Bayley, H. *Angew. Chem., Int. Ed.* **2015**, *54* (28), 8154−9.
(23) Zhou, S.; Wang, L.; Chen, X.; Guan, X. *ACS Sens* **2016**, *1* (5), 607−613.
(24) Gopfrich, K.; Li, C. Y.; Ricci, M.; Bhamidimarri, S. P.; Yoo, J.; Gyenes, B.; Ohmann, A.; Winterhalter, M.; Aksimentiev, A.; Keyser, U. F. *ACS Nano* **2016**, *10* (9), 8207−14.
(25) Hernandez-Ainsa, S.; Keyser, U. F. *Nanoscale* **2014**, *6* (23), 14121−32.
(26) Rofeh, J.; Schankweiler, S.; Morton, D.; Mortezaei, S.; Qiang, L.; Gundlach, J.; Fisher, J.; Theogarajan, L. *Appl. Phys. Lett.* **2019**, *114* (21), 213701.
(27) Morton, D.; Mortezaei, S.; Yemenicioglu, S.; Isaacman, M. J.; Nova, I. C.; Gundlach, J. H.; Theogarajan, L. *J. Mater. Chem. B* **2015**, *3* (25), 5080−5086.
(28) Vercoutere, W.; Winters-Hilt, S.; Olsen, H.; Deamer, D.; Haussler, D.; Akeson, M. *Nat. Biotechnol.* **2001**, *19* (3), 248−52.
(29) Maglia, G.; Heron, A. J.; Stoddart, D.; Japrung, D.; Bayley, H. *Methods Enzymol.* **2010**, *475*, 591−623.
(30) O'Shaughnessy, T. J.; Hu, J. E.; Kulp, J. L., 3rd; Daly, S. M.; Ligler, F. S. *Biomed. Microdevices* **2007**, *9* (6), 863−8.
(31) Mayer, M.; Kriebel, J. K.; Tosteson, M. T.; Whitesides, G. M. *Biophys. J.* **2003**, *85* (4), 2684−95.
(32) Zakharian, E. *Methods Mol. Biol.* **2013**, *998*, 109−18.
(33) Kalsi, S.; Powl, A. M.; Wallace, B. A.; Morgan, H.; de Planque, M. R. *Biophys. J.* **2014**, *106* (8), 1650−9.
(34) Nardin, C.; Winterhalter, M.; Meier, W. *Langmuir* **2000**, *16* (20), 7708−7712.
(35) Kumar, M.; Habel, J. E.; Shen, Y. X.; Meier, W. P.; Walz, T. *J. Am. Chem. Soc.* **2012**, *134* (45), 18631−7.
(36) Kowal, J.; Wu, D. L.; Mikhalevich, V.; Palivan, C. G.; Meier, W. *Langmuir* **2015**, *31* (17), 4868−4877.
(37) Wong, D.; Jeon, T.-J.; Schmidt, J. *Nanotechnology* **2006**, *17* (15), 3710−3717.
(38) Burden, D. L.; Kim, D.; Cheng, W.; Chandler Lawler, E.; Dreyer, D. R.; Burden, L. K. *Langmuir* **2018**, *34*, 10847.
(39) Jeon, T. J.; Malmstadt, N.; Schmidt, J. J. *J. Am. Chem. Soc.* **2006**, *128* (1), 42−3.
(40) Kang, X. F.; Cheley, S.; Rice-Ficht, A. C.; Bayley, H. *J. Am. Chem. Soc.* **2007**, *129* (15), 4701−5.
(41) Shim, J. W.; Gu, L. Q. *Anal. Chem.* **2007**, *79* (6), 2207−13.
(42) Malmstadt, N.; Jeon, L. J.; Schmidt, J. J. *Adv. Mater.* **2008**, *20* (1), 84.
(43) Jeon, T. J.; Malmstadt, N.; Poulos, J. L.; Schmidt, J. J. *Biointerphases* **2008**, *3* (2), FA96.
(44) White, R. J.; Ervin, E. N.; Yang, T.; Chen, X.; Daniel, S.; Cremer, P. S.; White, H. S. *J. Am. Chem. Soc.* **2007**, *129* (38), 11766−75.
(45) Hirano-Iwata, A.; Aoto, K.; Oshima, A.; Taira, T.; Yamaguchi, R. T.; Kimura, Y.; Niwano, M. *Langmuir* **2010**, *26* (3), 1949−52.
(46) Baker, C. A.; Bright, L. K.; Aspinwall, C. A. *Anal. Chem.* **2013**, *85* (19), 9078−86.
(47) Studer, A.; Demarche, S.; Langenegger, D.; Tiefenauer, L. *Biosens. Bioelectron.* **2011**, *26* (5), 1924−8.
(48) Tadaki, D.; Yamaura, D.; Araki, S.; Yoshida, M.; Arata, K.; Ohori, T.; Ishibashi, K. I.; Kato, M.; Ma, T.; Miyata, R.; Tozawa, Y.; Yamamoto, H.; Niwano, M.; Hirano-Iwata, A. *Sci. Rep.* **2017**, *7* (1), 17736.
(49) Liu, B.; Rieck, D.; Van Wie, B. J.; Cheng, G. J.; Moffett, D. F.; Kidwell, D. A. *Biosens. Bioelectron.* **2009**, *24* (7), 1843−9.
(50) Pang, Y.; Shu, Y.; Shavezipur, M.; Wang, X.; Mohammad, M. A.; Yang, Y.; Zhao, H.; Deng, N.; Maboudian, R.; Ren, T. L. *Sci. Rep.* **2016**, *6*, 28552.
(51) Nakane, J.; Akeson, M.; Marziali, A. *Electrophoresis* **2002**, *23* (16), 2592−2601.
(52) Maglia, G.; Restrepo, M. R.; Mikhailova, E.; Bayley, H. *Proc. Natl. Acad. Sci. U. S. A.* **2008**, *105* (50), 19720−5.
(53) Ding, Y.; Fleming, A. M.; White, H. S.; Burrows, C. J. *J. Phys. Chem. B* **2014**, *118* (45), 12873−82.
(54) Mathe, J.; Visram, H.; Viasnoff, V.; Rabin, Y.; Meller, A. *Biophys. J.* **2004**, *87* (5), 3205−12.
(55) Mathé, J.; Aksimentiev, A.; Nelson, D. R.; Schulten, K.; Meller, A. *Proc. Natl. Acad. Sci. U. S. A.* **2005**, *102* (35), 12377−12382.
(56) Meller, A.; Branton, D. *Electrophoresis* **2002**, *23* (16), 2583−2591.

DOI: 10.1021/acs.nanolett.9b04446
Nano Lett. 2019, 19, 9145−9153

(57) Henrickson, S. E.; Misakian, M.; Robertson, B.; Kasianowicz, J. J. *Phys. Rev. Lett.* **2000**, *85* (14), 3057.
(58) Wanunu, M.; Morrison, W.; Rabin, Y.; Grosberg, A. Y.; Meller, A. *Nat. Nanotechnol.* **2010**, *5* (2), 160−5.

DOI: 10.1021/acs.nanolett.9b04446
Nano Lett. 2019, 19, 9145−9153